



Short Communication

Humanized mice for investigating SARS-CoV-2 lung infection and associated human immune responses

Renren Sun^{#1}, Zongzheng Zhao^{#2} , Cong Fu¹, Yixin Wang^{1,3},
Zhendong Guo², Chunmao Zhang², Lina Liu⁴, Cheng Zhang⁵, Chang Shu¹,
Jin He¹, Yong-Guang Yang¹, Shucheng Hua^{1,3}, Yuwei Gao²
and Zheng Hu¹ 

¹ Key Laboratory of Organ Regeneration & Transplantation of Ministry of Education, and National-Local Joint Engineering Laboratory of Animal Models for Human Diseases, The First Hospital of Jilin University, Changchun, China

² Changchun Veterinary Research Institute, Chinese Academy of Agricultural Sciences, Changchun, China

³ Department of Respiration, The First Hospital of Jilin University, Changchun, China

⁴ College of Veterinary Medicine, Jilin University, Changchun, China

⁵ College of Veterinary Medicine, Hebei Agricultural University, Baoding, China

There is an urgent need for animal models of coronavirus disease 2019 to study immunopathogenesis and test therapeutic intervenes. In this study, we showed that NOD/SCID IL2rg^{-/-} (NSG) mice engrafted with human lung (HL) tissue (NSG-L mice) could be infected efficiently by severe acute respiratory syndrome coronavirus 2 (SARS-CoV-2), and that live virus capable of infecting Vero cells was found in the HL grafts and multiple organs from infected NSG-L mice. RNA-Sequencing identified a series of differentially expressed genes, which are enriched in viral defense responses, chemotaxis, IFN stimulation and pulmonary fibrosis, between HL grafts from infected and control NSG-L mice. Furthermore, when infected with SARS-CoV-2, humanized mice with both human immune system (HIS) and autologous HL grafts (HISL mice) had bodyweight loss and hemorrhage and immune cell infiltration in HL grafts, which were not observed in immunodeficient NSG-L mice, indicating the development of anti-viral immune responses in these mice. In support of this possibility, the infected HISL mice showed bodyweight recovery and lack of detectable live virus at the later time. These results demonstrate that NSG-L and HISL mice are susceptible to SARS-CoV-2 infection, offering a useful *in vivo* model for studying SARS-CoV-2 infection and the associated immune response and immunopathology, and testing anti-SARS-CoV-2 therapies.

Keywords: HISL mice · humanized mouse · lung infection · NSG mice · SARS-CoV-2



Additional supporting information may be found online in the Supporting Information section at the end of the article.

Correspondence: Dr. Shucheng Hua, Zheng Hu and Yuwei Gao
e-mail: shuchenghua@126.com; gaoyuwei@gmail.com;
zhenghu@jlu.edu.cn

[#]These authors contributed equally to this work.

Introduction

The lack of animal models that can be easily used to model severe acute respiratory syndrome coronavirus 2 (SARS-CoV-2) infection and pathogenesis in biosafety level 3/4 facilities is an important drawback factor impeding mechanistic understanding of coronavirus disease 2019 (COVID-19) pathogenesis and test new antiviral therapies [1]. Although mice are the most popular and easily handleable animal model, conventional murine models are not suitable for COVID-19 studies because most SARS-CoV-2 strains cannot use murine angiotensin-converting enzyme 2 (ACE2) to invade mouse cells [2]. Although mice with transgenic expression of human ACE2 were recently created and demonstrated to be susceptible to SARS-CoV-2 infection [3, 4], this model overlooks other proteins involved, such as transmembrane serine protease 2 (TMPRSS2) and CD147 [5, 6]. Mouse-adapted SARS-CoV-2 models provide useful platform for studying COVID-19 in mice [7, 8], but the profound evolutionary divergences between mice and humans also compromise their value to faithfully replicate viral infection process and the associated disorders [9]. Recently, Dr. Richard Flavell's group showed that humanized MISTRG6 mice that received human ACE-2 AAV injection can be infected by SARS-CoV-2 virus in lung-resident human macrophages and develop chronic immunoinflammatory features of COVID-19 while the lung microenvironment is still murine but not human [10]. Nonhuman primates are genetically close to human and can be infected by SARS-CoV-2 [11]; however, their wide usage is intensively restrained due to their extreme high cost and the need for complicated operating procedures, especially in biosafety level 3/4 facilities. Thus, there is an urgent need for novel animal models that are easy to handle and faithfully mimic human SARS-CoV-2 infection and the associated immune responses.

Immune surveillance plays crucial roles in the control of viral infection and the development of inflammatory syndromes, including pneumonia and cytokine storm in COVID-19 patients [12]. Previous studies of ours and other groups have shown that human immune system (HIS) mice made by co-transplantation of human fetal thymic tissue (under renal capsule) and CD34⁺ fetal liver cells (FLCs, i.v.) could mount antigen-specific human T and antibody responses following immunization, viral infections, or transplantation [13–16]. Recently, we generated an HIS mouse model with autologous human lung (HL) tissues (referred to as HISL) by transplantation of both human fetal lung (subcutaneous) and thymic tissues and CD34⁺ FLCs, and validated its efficacy to study HL resident immunity and antiviral response for H1N1 viral infection [17]. Herein, we further explored its application for SARS-CoV-2 infection investigation. We found that these HISL mice could be infected by SARS-CoV-2 virus and develop anti-viral immune responses, offering a convenient and useful in vivo model for understanding COVID-19 pathogenesis and testing anti-SARS-CoV-2 interventions.

Results and discussion

Entry and replication of SARS-CoV-2 in HL xenografts in mice

We first determined whether HL tissue grafted in NOD/SCID IL2rg^{-/-} (NSG) mice can be infected by SARS-CoV-2. Briefly, NSG mice were implanted subcutaneously with HL tissue (NSG-L mice), and subjected to infection via intra-HL injection of SARS-CoV-2 or PBS (as controls) 6–8 weeks later. Immunohistochemistry (IHC) examination confirmed human ACE2 protein expression throughout the HL xenografts (Fig. 1A). Real-time qPCR (RT-qPCR) analysis revealed that SARS-CoV-2 RNA was detected in HL and various mouse tissues including heart, liver, spleen, lung, kidney, brain, and intestine of NSG-L mice at days 1 and 3 following inoculation of 10⁶ 50% tissue culture infection dose (TCID₅₀) SARS-CoV-2, but not in NSG mice receiving subcutaneous injection of a similar number of virus (Fig. 1B), demonstrating SARS-CoV-2 infection and expansion in HL xenografts. To confirm this observation, another cohort of NSG-L mice was intra-HL inoculated with SARS-CoV-2 or PBS. Again, viral copies were detected in HL at days 3, 5, 8, 14, and 21 after infection (Fig. 1C). Importantly, 13 out of 14 HL homogenate samples (except one at day 21) harvested from SARS-CoV-2-infected NSG-L mice at days 3, 5, 8, 14, and 21 after infection retained the capability to re-infect Vero E6 cells in vitro, demonstrating the existence of live SARS-CoV-2 in HL xenografts (Fig. 1D). However, viral inoculation did not lead to significant bodyweight loss (Fig. 1E) or detectable pathological changes, such as tissue hemorrhage and lymphocyte infiltration, in HL grafts (Fig. 1F) or mouse tissues (Supporting Information Fig. 1), likely due to the immunodeficiency of NSG-L mice. This is in line with previous reports that the complications in COVID-19 patients are largely attributable to immune responses driven by SARS-CoV-2 infection [18]. These results demonstrate that NSG-L mice, which can be easily constructed and comfortably used in ABSL-3 laboratories, offer an effective in vivo model for identifying and comparing different viral strains and testing the efficacy of anti-viral drugs including neutralizing antibodies.

RNA sequencing analysis for HL xenografts after SARS-CoV-2 infection

To further understand the insight into SARS-CoV-2 infection induced changes in HL cells, we analyzed the transcriptome by RNA sequencing (RNA-seq) of HL samples from uninfected or SARS-CoV-2-infected NSG-L mice 5 and 21 days after SARS-CoV-2 inoculation. One randomly selected HL sample was analyzed for each of the three groups. For day 5 HL grafts, a total of 4612 human genes were differentially expressed between two samples, of which 2129 genes were significantly upregulated and 2483 genes were downregulated ($|\log_2(\text{FoldChange})| > 1$ & $p_{adj} < 0.05$) in SARS-CoV-2-infected compared to uninfected

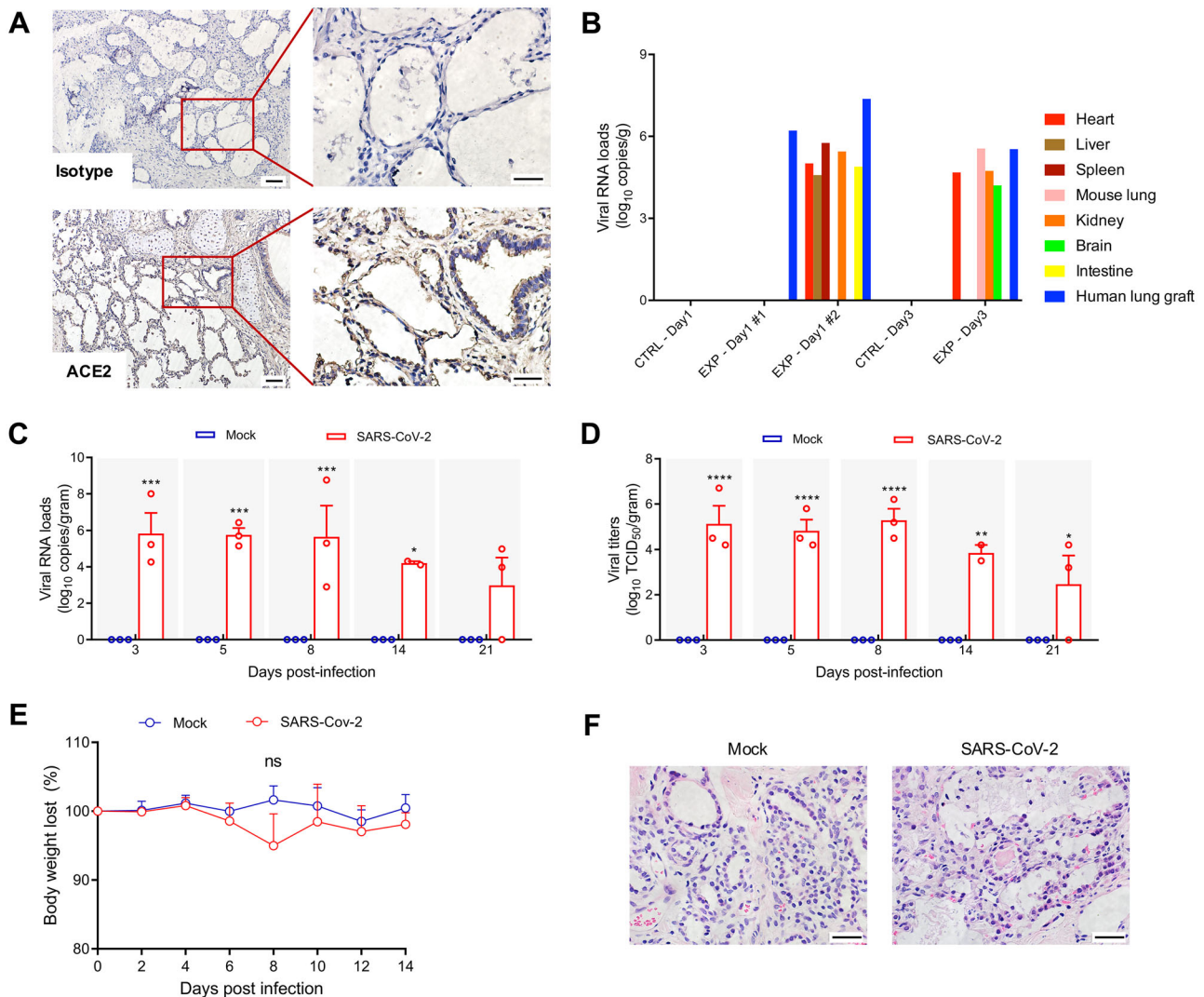


Figure 1. SARS-CoV-2 infection of HL xenografts in NSG mice. NSG-L mice were subjected to SARS-CoV-2 infection (10^6 TCID₅₀ given by intra-HL injection) 6–8 weeks after HL transplantation. Data from two independent experiments are presented, in which NSG mice receiving subcutaneous injection of SARS-CoV-2 (B) or NSG-L mice receiving intra-HL injection of PBS (C–F) were used as controls, respectively. (A) Representative IHC images of human lung xenograft sections from six NSG-L mice stained with human ACE2 (lower panel) or isotype control (upper panel). scale bar (left panel) = 50 μ m; scale bar (right panel) = 20 μ m. (B) Viral copies in the indicated tissues examined by RT-qPCR 1 or 3 days after infection. Data are from two NSG-L mice for SARS-CoV-2-infected group (EXP-Day1 #1 and EXP-Day1 #2; NSG-L mice receiving intra-HL injection of SARS-CoV-2) and one NSG mouse for control group (CTRL-Day1; NSG mouse receiving subcutaneous injection of SARS-CoV-2) at day 1, and one NSG-L mice for SARS-CoV-2-infected group (EXP-Day3; NSG-L mouse receiving intra-HL injection of SARS-CoV-2) and one NSG mouse for control group (CTRL-Day3; NSG mouse receiving subcutaneous injection of SARS-CoV-2) at day 3. (C) Viral RNA was examined by RT-qPCR in HL xenografts at days 3, 5, 8, 14, and 21 after infection (each symbol represents an individual animal). A standard curve was fitted using a series of 10-fold dilutions of a standard plasmid DNA of SARS-CoV-2, and the number of the viral RNA copies in HL samples was estimated from the measured cycle threshold (Ct) values. (D) Viral titers were measured by Vero E6 cells in HL xenografts at days 3, 5, 8, 14, and 21 after infection (each symbol represents an individual animal). (E) Bodyweight changes at the indicated time points after NSG-L mice were intra-HL inoculated with SARS-CoV-2 or PBS. Data are from three mice per group at each time points. (F) Representative H&E images of HL xenografts at day 5 after intra-HL injection of PBS (left panel, $n = 3$) or SARS-CoV-2 (right panel, $n = 3$), scale bar = 20 μ m. Data are shown as mean values \pm SEM. ns, no significant difference, * $p < 0.05$, ** $p < 0.01$, *** $p < 0.001$, **** $p < 0.0001$ (by two-way analysis of variance [ANOVA] analysis–Sidak’s multiple comparisons test).

HL grafts (Fig. 2A, left panel). For day 21 HL grafts, a total of 6488 human genes were differentially expressed between the two samples, of which 3311 and 3177 genes were significantly upregulated and downregulated ($|\log_2(\text{FoldChange})| > 1$ & $\text{padj} < 0.05$), respectively, in SARS-CoV-2-infected compared to uninfected HL grafts (Fig. 2A, right panel). Many of these differentially expressed genes are associated with viral defense

responses, including NLRC5, MICB, APOBEC3D, APOBEC3G, IFI6, ISG15, and IFITM3, which were markedly upregulated in infected HL grafts at days 5 and 21 compared to HL grafts from uninfected NSG-L mice (Fig. 2B). Notably, HL grafts from the infected NSG-L mice showed a great upregulation of viral infection-associated chemokines (e.g., CCL11 and CXCL6 at day 5, and CCL19, CXCL19, CXCL13, CCL18 at day 21; Fig. 2C) and

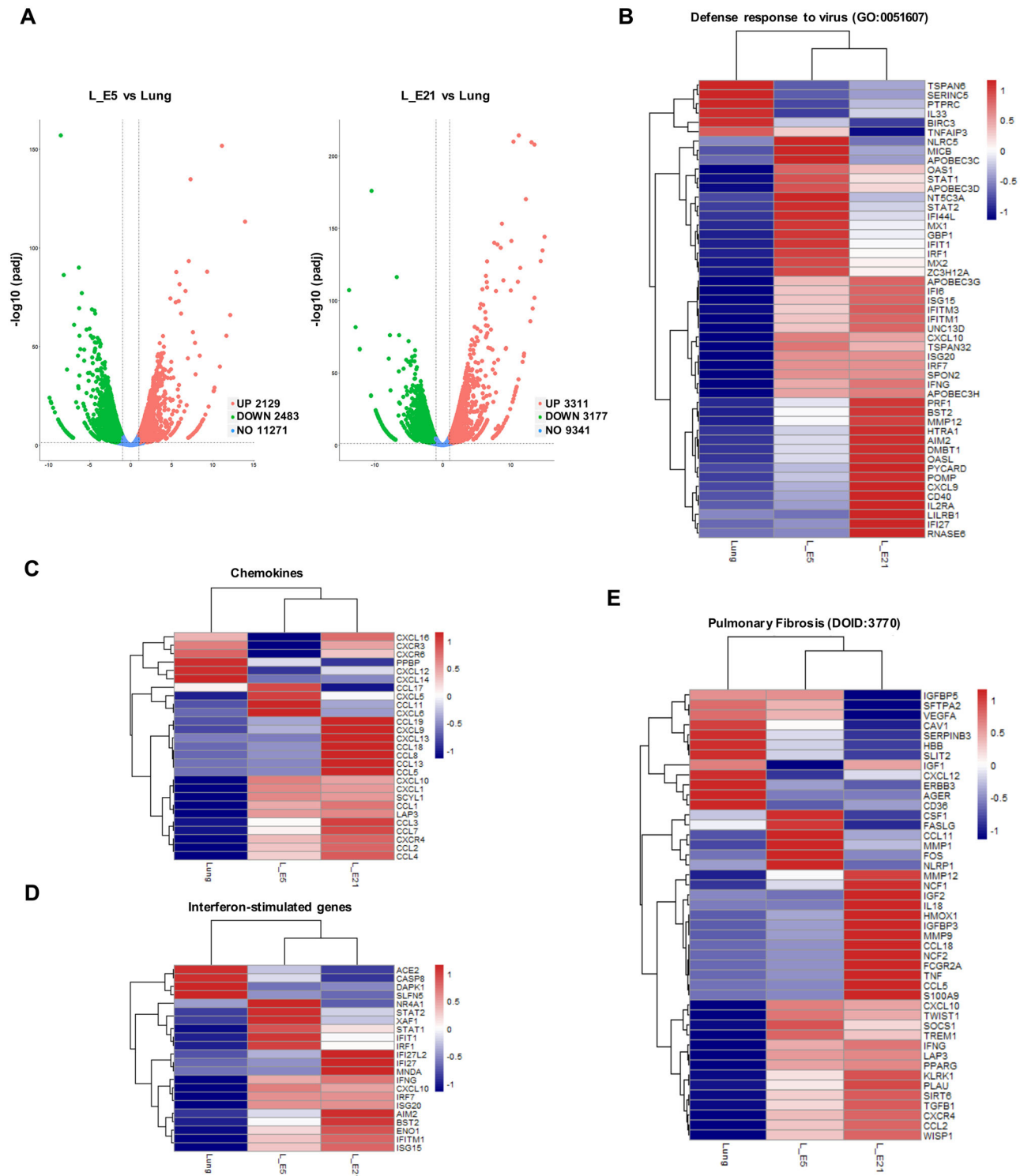


Figure 2. RNA-seq analysis for HL grafts from NSG-L mice after SARS-CoV-2 infection. HL grafts injected with 10^6 TCID₅₀ SARS-CoV-2 virus were harvested from NSG-L mice for RNA-seq examination at day 5 and 21 after infection; Naïve HL graft without infection was used as control. (A) Volcano plot showing differentially expressed genes (DEGs) of HL grafts for SARS-CoV-2-infected and noninfected NSG-L mice at day 5 (left panel) or day 21 (right panel). The data for all genes are plotted as \log_2 fold change versus the $-\log_{10}$ of the adjusted p -value. (B–E) Heatmaps of RNA-seq expression Z-scores computed for selected genes that are differentially expressed ($p_{adj} < 0.05$, $|\log_2(\text{foldchange})| > 1$) between three pairwise comparisons (L_E5 vs. L_E21, Lung vs. L_E5, Lung vs. L_E21). (B) Heatmap of DEGs under gene ontology (GO) term “Defense response to virus” (BP GO: 0051607); (C) DEGs related to chemokines; (D) DEGs related to IFN-stimulated genes; (E) heatmap of DEGs under disease ontology (DO) term “Pulmonary Fibrosis” (DOID:3770). RNA-Seq examination was performed once and each group contained one randomly selected HL sample.

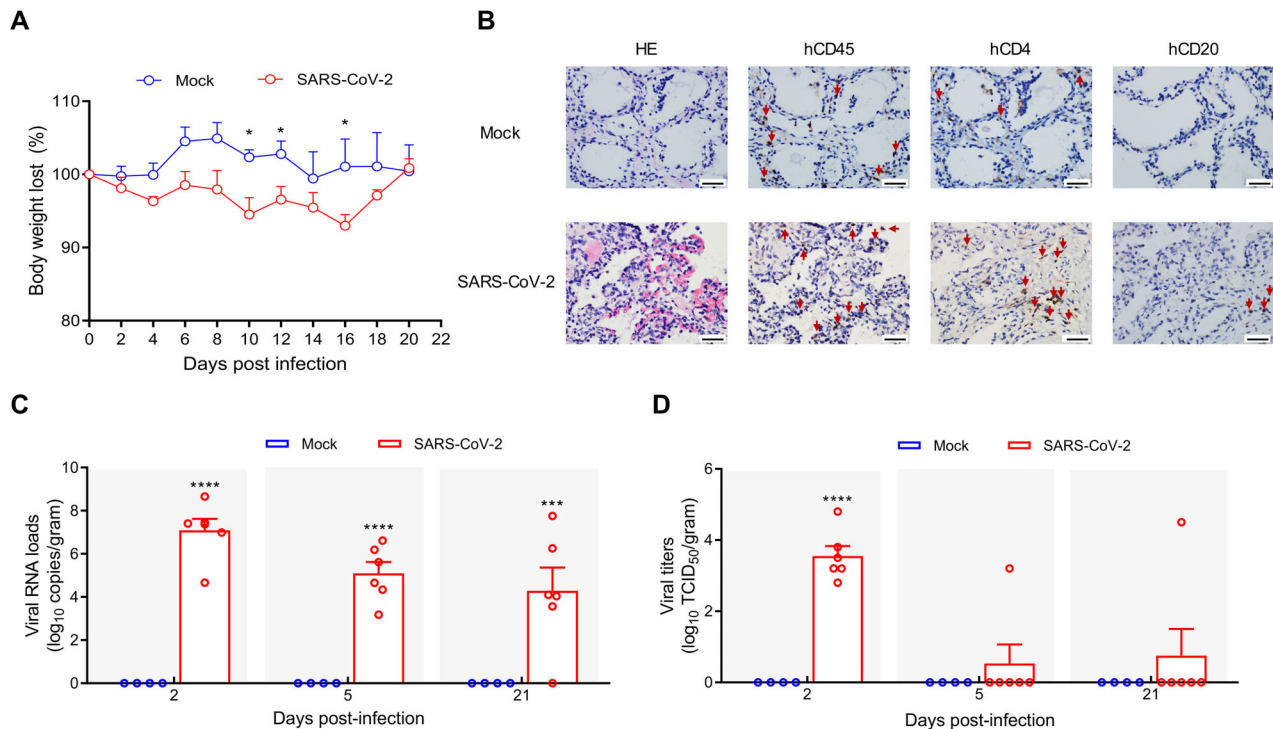


Figure 3. HISL mice are susceptible for SARS-CoV-2. HISL mice were constructed by co-transplantation of HL (subcutaneously), thymic tissues (under renal capsule) and CD34⁺ FLCs (i.v.), and subjected to intra-HL inoculation of 10^6 TCID₅₀ SARS-CoV-2 or PBS at week 17 post-humanization. (A) Bodyweight changes of HISL mice infected with SARS-CoV-2 ($n = 6$) or PBS ($n = 4$) at day 5. (B) Representative H&E and IHC images of human lung sections of HISL mice infected with SARS-CoV-2 ($n = 6$) or PBS ($n = 4$) at day 5, scale bar = 20 μ m. (C) Mice were euthanized at days 2, 5, and 21 after infection, and SARS-CoV-2 viral copies were examined by RT-qPCR. A standard curve was fitted using a series of 10-fold dilutions of a standard plasmid DNA of SARS-CoV-2, and the number of the viral RNA copies was estimated from the measured cycle threshold (Ct) values. (D) Viral titers were measured by Vero E6 cells in HL xenografts at days 2, 5, and 21 after infection (each symbol represents an individual animal). Data are shown as mean values \pm SEM of a single experiment (SARS-CoV-2, $n = 6$; Mock, $n = 4$). * $p < 0.05$, ** $p < 0.01$, *** $p < 0.001$, **** $p < 0.0001$ (by two-way analysis of variance [ANOVA] analysis–Sidak’s multiple comparisons test)

interferon-stimulated genes (ISGs; e.g., IFIT1 and STAT1 at day 5, and ISG15, IFITM1, and IFI27 at day 21; Fig. 2D) compared to those from noninfected NSG-L mice. Furthermore, SARS-CoV-2 infection induced intensive upregulation of genes involved in pulmonary fibrosis at day 5 (e.g., CSF1, FASLG, NLRP1) and day 21 (e.g., IGF2, IL18, MMP9) in infected HL grafts (Fig. 2E), providing a mechanistic explanation for the reported development of lung fibrosis, a long-term and presumably irreversible complication of COVID-19 patients [19]. Additionally, SARS-CoV-2-infected HL also showed upregulation in transforming growth factor β (TGF β) gene at day 21 (Fig. 2E), which was in line with the recent findings that higher serum levels of TGF β is a hallmark of severe COVID-19 [20]. These data support the use of NSG-L mice as a convenient and useful in vivo model to study the kinetic changes in gene expression profiles caused by interaction between SARS-CoV-2 and HL parenchymal cells.

Development of antiviral immunity in HISL mice following SARS-CoV-2 infection

We next examined SARS-CoV-2 infection in HISL mice with both HL and human immunity. Briefly, HISL mice were constructed

by transplantation of HL and thymic tissues and CD34⁺ cells, and subjected to SARS-CoV-2 infection after human immune reconstitution was confirmed by measuring human immune cells in peripheral blood. FACS analysis of PBMCs 14 weeks after humanization detected high levels of human CD45⁺ lymphohematopoietic cells composed of CD3⁺ T cells (including both CD4 and CD8 T cells), CD20⁺ B cells, and CD33⁺ myeloid cells in HISL mice (Supporting Information Fig. 2A). Furthermore, human CD45⁺ immune cells including CD4⁺ T cells, CD20⁺ B cells, and CD11c⁺ dendritic cells were also detected in spleen and HL grafts from these mice (Supporting Information Fig. 2B). These HISL mice were randomly divided into two groups and infected 3 weeks later with SARS-CoV-2 or PBS as controls. Unlike NSG-L mice (Fig. 1), HISL mice showed a significant bodyweight loss after intra-HL SARS-CoV-2 infection, which returned to a level comparable to the control HISL mice by 21 days (Fig. 3A). Graft-versus-host disease syndrome was not observed before or during SARS-CoV-2 infection, which excludes its influence for mouse bodyweight changes. No mortality was observed in HISL mice infected with SARS-CoV-2. Furthermore, HL grafts from HISL mice that received SARS-CoV-2 (but not PBS) had hemorrhage at day 5, which was associated with increased infiltration of human CD45⁺ cells, including CD4⁺ T (1703 ± 238 cells/mm²

in SARS-CoV-2-infected HL compared with 645 ± 80 cells/mm² in mock-infected HL) and CD20⁺ B cells (189 ± 22 cells/mm² in SARS-CoV-2-infected HL compared with 86 ± 14 cells/mm² in mock-infected HL) (Fig. 3B). Although the levels of human T- and B-cell infiltration in HL grafts became comparable between the two groups at day 21, there were still significantly more human CD33⁺ myeloid cells (Supporting Information Fig. 3A), including CD11c⁺ cells (Supporting Information Fig. 3B), in HL grafts in SARS-CoV-2-infected than mock-infected mice, which is in line with previous reports for patients [21]. No significant difference was detected for any human immune cell populations in WBCs, including CD3⁺ T, CD20⁺ B, CD33⁺ myeloid, and CD56⁺ NK cells between SARS-CoV-2- and mock-infected mice at day 21 (Supporting Information Fig. 3C). Viral copies were detected by RT-qPCR in all HL samples (except one at day 21) from SARS-CoV-2-infected HISL mice, but not those from the control HISL mice (Fig. 3C). However, in contrast to HL homogenates from infected NSG-L mice (Fig. 1), HL homogenate samples from most infected HISL mice harvested at day 5 (5 out of 6) and day 21 (5 out of 6) failed to infect Vero E6 cells in vitro (Fig. 3D), indicating an efficient elimination of live SARS-CoV-2 by HIS in these mice. Therefore, these results support the use of HISL mice to study COVID-19 pathogenesis and anti-SARS-CoV-2 immunotherapy.

Concluding remarks

In this study, we established a humanized mouse model carrying HL tissue and autologous HIS, which can be easily constructed and comfortably used in ABSL-3 laboratories. We found that these humanized mice are susceptible to infection by SARS-CoV-2 and develop disease-associated lung injury. Although not capable of modeling upper respiratory or systemic infection/manifestations, as only the HL xenograft is susceptible to SARS-CoV-2 in these mice, the HISL mouse model is still a useful model that permits in vivo assessment of human immune responses against SARS-CoV-2 infection. Together, the NSG-L (with HL tissue implantation) and HISL (with both HL tissue implantation and immune system reconstitution) humanized mouse model offer convenient and powerful in vivo models for evaluating the immunopathology of COVID-19 and the efficacy of anti-viral immunotherapies, such as vaccination.

Material and methods

Mice and human tissues

NOD-Prkd^{cem26Cd52}Il2rg^{em26Cd22}/Nju (referred to as NSG) mice were purchased from Nanjing Biomedical Research Institute of Nanjing University. Female mice were used in the experiments between 6–8 weeks of age, and they were housed in a specific pathogen-free microisolator environment. Discard human fetal samples of gestational age of 17–20 weeks were obtained with

informed consent at the First Hospital of Jilin University. Human fetal thymic and lung tissues were cut into small pieces with a diameter of around 1 or 5 mm, respectively, and CD34⁺ human hematopoietic stem/progenitor cells were purified from FLCs by magnetic-activated cell sorting (MACS; with a purity of >90% confirmed by FACS). The human tissues and cells were cryopreserved in liquid nitrogen until use.

NSG-L and HISL humanized mouse model construction

NSG-L mice were made by subcutaneous implantation of human fetal lung tissue (approximately 5 mm in diameter). HISL humanized mice were made by implantation of human fetal thymic tissue (around 1 mm in diameter; under the renal capsule) and lung tissue (5 mm in diameter; subcutaneously) in NSG mice that pre-conditioned with 1.75 Gy total body irradiation (Rad Source RS2000pro-225, USA), followed by intravenous injection of $1\text{--}2 \times 10^5$ human CD34⁺ FLCs (given 6–8 h after irradiation).

Flow cytometric analysis

Mouse PBMCs were prepared using density gradient centrifugation with Histopaque 1077 (Sigma-Aldrich, St. Louis, MO, USA). Single-cell suspensions of human and mouse lung tissues were prepared by digestion using 0.1 mg/mL collagenase Type IV (Thermo Fisher Scientific, MA, USA) and 0.01 mg/mL DNase I (Sigma-Aldrich) at 37°C for 40 min. Human immune cell reconstitution in humanized mice were determined by flow cytometry using following fluorochrome-conjugated antibodies: anti-human CD45, CD3, CD4, CD8, CD20, CD33, CD56; anti-mouse CD45 and Ter119 (BD Biosciences, USA). Examination was performed on a Cytek Aurora Flow cytometer (Cytek Biosciences, USA), and data were analyzed using the FlowJo software version 10.6.2. Dead cells were excluded from the analysis by gating out PI retaining cells.

SARS-CoV-2 virus preparation and titer determination

SARS-CoV-2 (BetaCoV/Beijing/IME-BJ05-2020) was passaged in Vero E6 cells, which are maintained in Dulbecco's modified Eagle's medium (DMEM; Invitrogen, Carlsbad, CA, USA) with supplemented 2% fetal bovine serum (FBS; Gibco, Auckland, New Zealand). Viral titers were determined using a standard TCID₅₀ assay.

Mouse experiments

NSG-L or HISL mice were anesthetized with isoflurane and injected with 100 μL of 10^6 TCID₅₀ of SARS-CoV-2 or PBS into the HL graft. The mice were followed for bodyweight changes, and

euthanized for measuring viral particles and histological changes in HL grafts and tissues at indicated time points.

RNA extraction and RT-qPCR

Total RNA was extracted from tissues homogenates using the RNeasy Mini Kit (Qiagen, Hilden, Germany), and viral RNA loads were determined by a SARS-CoV-2 RNA detection kit (Shenzhen Puruikang Biotech, China). The viral RNA loads for the target SARS-CoV-2 N gene was normalized to the standard curve obtained by using a plasmid containing the full-length cDNA of the SARS-CoV-2 N gene. The reactions were performed with CFX96 system (BIO-RAD, USA) according to the following protocol: 50°C for 20 min for reverse transcription, followed by 95°C for 3 min and then 45 cycles of 95°C for 5 s, 56°C for 45 s. Results were presented as log₁₀ numbers of genome equivalent copies per gram of sample.

Histology

Tissues were embedded in paraffin, and sectioned (2.5 μm) for H&E and IHC examination. For IHC, tissue sections were first stained with monoclonal anti-human CD45 (DAKO, 2B11+PD7/26), CD4 (Abclonal; ARC0328), CD20 (DAKO, L26), or CD11c (Abcam; EP1347Y), and ACE2 (Abcam; EPR4435(2)) antibodies, and the immunoreactivity was detected with UltraSensitive™ Streptavidin-Peroxidase Kit (KIT-9710, Mai Xin, China) according to the manufacturer's protocol.

RNA-seq

Total RNA was polyA-selected, fragmented, and the samples were examined on an Illumina Novaseq6000 machine, yielding an average of 22 million uniquely aligned paired-end 150-mer reads per sample. Reads were aligned with STAR RNA-seq aligner (Version 2.7.3a) using the UCSC/hg38 genome assembly and transcript annotation [22]. Expression levels were calculated as Fragments per Kilobase of transcript per Million reads (FPKM) using Cufflinks software [23]. Differential expression analysis was performed using Cuffdiff (version 2.2.1.Linux_x86_64) [23]. In each analysis, genes with thresholds of $|\log_2(\text{foldchange})| > 1$, $p_{adj} < 0.05$ and a mean FPKM value of more than 5 were tested. “Cluster Profiler” package (Release 3.16.1) [24] and “DOSE” package (Release 3.14.0) [25] in R software (version 4.0.2) was used for functional enrichment analysis, and gene ontology biological processes terms at the significant level (q -value < 0.05) were employed.

Statistical analysis

Data were analyzed using GraphPad Prism 8 software (San Diego, CA, USA) and presented as mean values \pm SEM. Immunohistochemical data were analyzed using Image J software (Bethesda,

MD, USA). The results were compared statistically using unpaired two-tailed Student's t test for the comparison of two groups and two-way analysis of variance with Sidak's posttest for multiple comparison. A p value of ≤ 0.05 was considered significant.

Acknowledgements: This work was supported by grants from NSFC (82001697, 81870091, U20A20342), Science Development Project of Jilin province (20190201295JC and 20200703012ZP), and special grants for COVID-19 research of Jilin province (20200901006SF).

Conflict of interest: The authors declare no commercial or financial conflict of interest.

Ethics statement: Protocols involved in the use of human samples and animals were reviewed and approved by the Institutional Review Board and Institutional Animal Care and Use Committee of the First Hospital of Jilin University, and all experiments with SARS-CoV-2 (COVID-19) were performed in biosecurity level 3 laboratory according to the protocols approved by the Changchun Veterinary Research Institute, Chinese Academy of Agricultural Sciences.

Author contributions: Z.H., Y-W. G., S-C.H., and Y-G.Y. conceived the study; R-R.S., Z-Z.Z., Y-X.W., C.S., and J.H. performed the experiments; C.F. contributed to RNA-seq data analysis; Z.H., Y-W.G., and S-C.H. supervised the work; Z.H., R-R.S., Z-Z.Z., C.F., and Y-G.Y. analyzed the data and wrote the manuscript; all authors edited and approved the manuscript.

Peer review: The peer review history for this article is available at <https://publons.com/publon/10.1002/eji.202249804>

Data availability statement: The data that support the findings of this study are openly available in the National Center for Biotechnology Information (NCBI) Gene Expression Omnibus (GEO) at <https://www.ncbi.nlm.nih.gov/geo/query/acc.cgi?acc=GSE175900>, reference number GSE175900.

References

- Muñoz-Fontela, C., Dowling, W.E., Funnell, S.G., Gsell, P.-S., Riveros-Balta, A.X., Albrecht, R.A., Andersen, H. et al., Animal models for COVID-19. *Nature* 2020. 586: 509–515.
- Wang, Q., Zhang, Y., Wu, L., Niu, S., Song, C., Zhang, Z., Lu, G. et al., Structural and functional basis of SARS-CoV-2 entry by using human ACE2. *Cell* 2020. 181: 894–904.e9.
- Bao, L., Deng, W., Huang, B., Gao, H., Liu, J., Ren, L., Wei, Q. et al., The pathogenicity of SARS-CoV-2 in hACE2 transgenic mice. *Nature* 2020. 583: 830–833.
- Zhao, M.-M., Yang, W.-L., Yang, F.-Y., Zhang, L., Huang, W.-J., Hou, W., Fan, C.-F. et al., Cathepsin L plays a key role in SARS-CoV-2 infection

- in humans and humanized mice and is a promising target for new drug development. *Signal Transduct. Target Ther.* 2021. **6**: 1–12.
- 5 Qiao, J., Li, W., Bao, J., Peng, Q., Wen, D., Wang, J., Sun, B. et al., The expression of SARS-CoV-2 receptor ACE2 and CD147, and protease TMPRSS2 in human and mouse brain cells and mouse brain tissues. *Biochem. Biophys. Res. Commun.* 2020. **533**: 867–871.
 - 6 Wang, K., Chen, W., Zhang, Z., Deng, Y., Lian, J.-Q., Du, P., Wei, D. et al., CD147-spike protein is a novel route for SARS-CoV-2 infection to host cells. *Signal Transduct. Target Ther.* 2020. **5**: 1–10.
 - 7 Dinnon, K.H., Leist, S.R., Schäfer, A., Edwards, C.E., Martinez, D.R., Montgomery, S.A., West, A. et al., A mouse-adapted model of SARS-CoV-2 to test COVID-19 countermeasures. *Nature* 2020. **586**: 560–566.
 - 8 Huang, K., Zhang, Y., Hui, X., Zhao, Y., Gong, W., Wang, T., Zhang, S. et al., Q493K and Q498H substitutions in Spike promote adaptation of SARS-CoV-2 in mice. *EBioMedicine.* 2021. **67**: 103381.
 - 9 Perrin, S., Preclinical research: Make mouse studies work. *Nature* 2014. **507**: 423–425.
 - 10 Sefik, E., Qu, R., Junqueira, C., Kaffe, E., Mirza, H., Zhao, J., Brewer, J.R. et al., Inflammasome activation in infected macrophages drives COVID-19 pathology. *Nature* 2022. **606**: 585–593.
 - 11 Blair, R.V., Vaccari, M., Doyle-Meyers, L.A., Roy, C.J., Russell-Lodrigue, K., Fahlberg, M., Monjure, C.J. et al., Acute respiratory distress in aged, SARS-CoV-2-infected African green monkeys but not rhesus macaques. *Am. J. Pathol.* 2021. **191**: 274–282.
 - 12 Sariol, A. and Perlman, S., Lessons for COVID-19 immunity from other coronavirus infections. *Immunity* 2020. **53**: 248–263.
 - 13 Lan, P., Tonomura, N., Shimizu, A., Wang, S. and Yang, Y.-G., Reconstitution of a functional human immune system in immunodeficient mice through combined human fetal thymus/liver and CD34+ cell transplantation. *Blood* 2006. **108**: 487–492.
 - 14 Tonomura, N., Habiro, K., Shimizu, A., Sykes, M. and Yang, Y.-G., Antigen-specific human T-cell responses and T cell-dependent production of human antibodies in a humanized mouse model. *Blood* 2008. **111**: 4293–4296.
 - 15 Tonomura, N., Shimizu, A., Wang, S., Yamada, K., Tchipashvili, V., Weir, G.C., Yang, Y.G. et al., Pig islet xenograft rejection in a mouse model with an established human immune system. *Xenotransplantation* 2008. **15**: 129–135.
 - 16 Brainard, D.M., Seung, E., Frahm, N., Cariappa, A., Bailey, C.C., Hart, W.K., Shin, H.-S. et al., Induction of robust cellular and humoral virus-specific adaptive immune responses in human immunodeficiency virus-infected humanized BLT mice. *J. Virol.* 2009. **83**: 7305–7321.
 - 17 Wang, Y., Wang, L., Fu, C., Wang, X., Zuo, S., Shu, C., Shan, Y. et al., Exploration of human lung-resident immunity and response to respiratory viral immunization in a humanized mouse model. *J. Immunol.* 2022. **208**: 420–428.
 - 18 Vardhana, S.A. and Wolchok, J.D., The many faces of the anti-COVID immune response. *J. Exp. Med.* 2020. **217**: 6.
 - 19 Grillo, F., Barisone, E., Ball, L., Mastracci, L. and Fiocca, R., Lung fibrosis: an undervalued finding in COVID-19 pathological series. *Lancet Infect. Dis.* 2021. **21**: e72.
 - 20 Witkowski, M., Tizian, C., Ferreira-Gomes, M., Niemeyer, D., Jones, T.C., Heinrich, F., Frischbutter, S. et al., Untimely TGF β responses in COVID-19 limit antiviral functions of NK cells. *Nature* 2021. **600**: 295–301.
 - 21 Szabo, P.A., Dogra, P., Gray, J.I., Wells, S.B., Connors, T.J., Weisberg, S.P., Krupska, I. et al., Longitudinal profiling of respiratory and systemic immune responses reveals myeloid cell-driven lung inflammation in severe COVID-19. *Immunity* 2021. **54**: 797–814. e6.
 - 22 Dobin, A., Davis, C.A., Schlesinger, F., Drenkow, J., Zaleski, C., Jha, S., Batut, P. et al., STAR: ultrafast universal RNA-seq aligner. *Bioinformatics* 2013. **29**: 15–21.
 - 23 Trapnell, C., Williams, B.A., Pertea, G., Mortazavi, A., Kwan, G., Van Baren, M.J., Salzberg, S.L. et al., Transcript assembly and quantification by RNA-Seq reveals unannotated transcripts and isoform switching during cell differentiation. *Nat. Biotechnol.* 2010. **28**: 511–515.
 - 24 Yu, G., Wang, L.-G., Han, Y. and He, Q.-Y., clusterProfiler: an R package for comparing biological themes among gene clusters. *Omic: J. Integr. Biol.* 2012. **16**: 284–287.
 - 25 Yu, G., Wang, L.-G., Yan, G.-R. and He, Q.-Y., DOSE: an R/Bioconductor package for disease ontology semantic and enrichment analysis. *Bioinformatics* 2015;31: 608–609.
- Abbreviations:** FLC: fetal liver cell · HL: human lung · NSG-L: NSG mice engrafted with human lung tissue · HIS: human immune system · SARS-CoV-2: severe acute respiratory syndrome coronavirus 2 · COVID-19: coronavirus disease 2019 · ACE2: angiotensin-converting enzyme 2 · IHC: immunohistochemistry · RT-qPCR: Real-time qPCR · RNA-seq: RNA sequencing · TCID₅₀: 50% tissue culture infection dose
- Full correspondence:** Dr. Shucheng Hua, Key Laboratory of Organ Regeneration & Transplantation of Ministry of Education, and National-Local Joint Engineering Laboratory of Animal Models for Human Diseases, Department of Respiration, The First Hospital of Jilin University, Changchun 130062, China
e-mail: shuchenghua@126.com
Yuwei Gao, Changchun Veterinary Research Institute, Chinese Academy of Agricultural Sciences, Changchun 130122, China
e-mail: gaoyuwei@gmail.com
Zheng Hu, Key Laboratory of Organ Regeneration & Transplantation of Ministry of Education, and National-Local Joint Engineering Laboratory of Animal Models for Human Diseases, The First Hospital of Jilin University, Changchun 130062, China
e-mail: zhenghu@jlu.edu.cn

Received: 10/1/2022

Revised: 23/6/2022

Accepted: 8/8/2022

Accepted article online: 17/8/2022